ROYAL NORWEGIAN COUNCIL FOR SCIENTIFIC AND INDUSTRIAL RESEARCH

PROCEEDINGS FROM THE SEMINAR ON

SEISMOLOGY AND SEISMIC ARRAYS

OSLO, 22–25 NOVEMBER 1971

Editors: E S Husebye and H Bungum

Arranged in connection with the opening of The Norwegian Seismic Array (NORSAR) 1972

PRELIMINARY RESULTS FROM THE NORSAR SHORT-PERIOD SYSTEM

C.P. FELIX, W.L. GILBERT AND S.G. WHEELER

IBM Federal Systems Division
Gaithersburg, Maryland

INTRODUCTION

Recent studies of NORSAR short-period data have been conducted by IBM for the following purposes:

- to evaluate the performance of the NORSAR short-period system,
- to obtain a better understanding of NORSAR seismic noise and signal characteristics in order to evaluate their effects on system performance, and
- to investigate various digital filters, detection techniques and other computational algorithms for processing NORSAR data.

This paper will report on certain aspects of these studies, including a preliminary estimate of NORSAR system performance (Anonymous, 1972a), and results which describe the nature and variety of NORSAR signal and noise characteristics (Anonymous, 1972b, c).

The data considered in Anonymous (1972b) consists of signal waveforms for 36 seismic events detected and recorded by the Interim NORSAR system (individual sensors from 18 subarrays) during early 1970, as well as noise data immediately preceding each of these events. Another study of signal and noise characteristics (Anonymous, 1972c) utilized subarray and array beam signal waveforms for 48 seismic events detected and recorded by the full NORSAR system (22 six-sensor subarrays) during the first half of 1971, as well as noise data preceding these events. The system performance estimates reported by Anonymous (1972a) have been derived from selected portions of the Detection Processor and Event

Processor outputs for the first half of 1971, and event magnitude bias estimates based on comparisons between NORSAR and U.S. National Ocean Survey (NOS) seismic event reports have also been obtained using data processed during this period.

In general, the results of these studies agree with previous observations by various investigators (Anonymous, 1968, and Toksöz, 1972) and serve to confirm their conclusions. However, the great variety of the seismic signals and background noise spectral characteristics which have been observed at NORSAR should be emphasized, and general conclusions drawn from data sets which are restricted with respect to time, azimuth or distance should be avoided. The results which are presented below exhibit some of this variety, but it will be necessary to analyze a considerably larger volume of data before the extremes of the signal and noise characteristics are well understood.

NOISE CHARACTERISTICS

Noise power spectral density functions have been estimated for individual short-period channels, subarray beams and array beams. These estimates have been obtained by application of the fast Fourier transform to either 32 or 64 sample blocks of 10 Hz sampled noise data, and by averaging of the power spectral density estimates at each frequency over several such time blocks to reduce the variability of the estimates. In addition, in order to reduce the effects of "spectral leakage" from strong frequencies to weak frequencies, digital filters have been applied to the original data and compensated for in the final estimates. This technique has been applied using a variety of digital filters (from seven to sixteen for each spectral density function) each of which is intended to emphasize some specific portion of the frequency band from zero to five Hz.

A comparison of the average power spectral density estimates across either the individual seismometer data channels or the subarray beams with the power spectral density function estimated for the array beam shows that the background noise is almost completely incoherent among subarrays, and nearly incoherent among instruments within a subarray, at all observed frequencies. That is, the noise power reduction due to beamforming at each frequency is approximately 10 $\log_{10} N$ dB, where N is the number of channels utilized in the beamforming operation.

Figure 1 shows a set of seven NORSAR noise power spectral density estimates which have been selected to exhibit the variety of spectral density functions which have been observed. Each of these seven functions has been computed by averaging the spectral density functions across all subarrays, and the results are presented in dB relative to one nm^2/Hz referenced to the output of an individual short-period data channel. The results are not compensated for the response characteristics of the short-period seismometer and data channel. Note that there is a variation in background noise level of from 10 dB to 15 dB at almost all frequencies, and that the variation of the high frequency portion (e.g., from two to five Hz) appears to be somewhat independent of the variation of the low frequency portion (e.g., from zero to 1.5 Hz).

Fig 2 shows five LASA noise power spectral density estimates which have been computed in the same way as the NORSAR noise spectra in Fig 1. Although these five curves do not represent the extreme variations in noise spectra which have been observed at LASA, they are reasonably typical. For comparison, Fig 3 shows two of the most extreme NORSAR noise spectra (nos. 2 and 6 from Fig 1) on the same plot as a typical LASA noise spectral density function (no. 4 from Fig 2). These curves indicate that the NORSAR seismic noise levels may be either higher or lower than those at LASA at either the extreme high or low end of the zero to five Hz frequency band. However, from about 0.9 Hz to approximately 1.8 Hz, the LASA noise is generally lower, and at times this difference is in excess of ten dB. This fact has unfortunate consequences for NORSAR signal processing, since the short-period channel response peaks at approximately 1.0 Hz and a significant portion of the energy of most signal waveforms is contained in this frequency band.

Fig 4 shows the average noise level observed on 331 array beams in the NORSAR Detection Processor over a period of approximately four days. This represents the noise level at the output of the

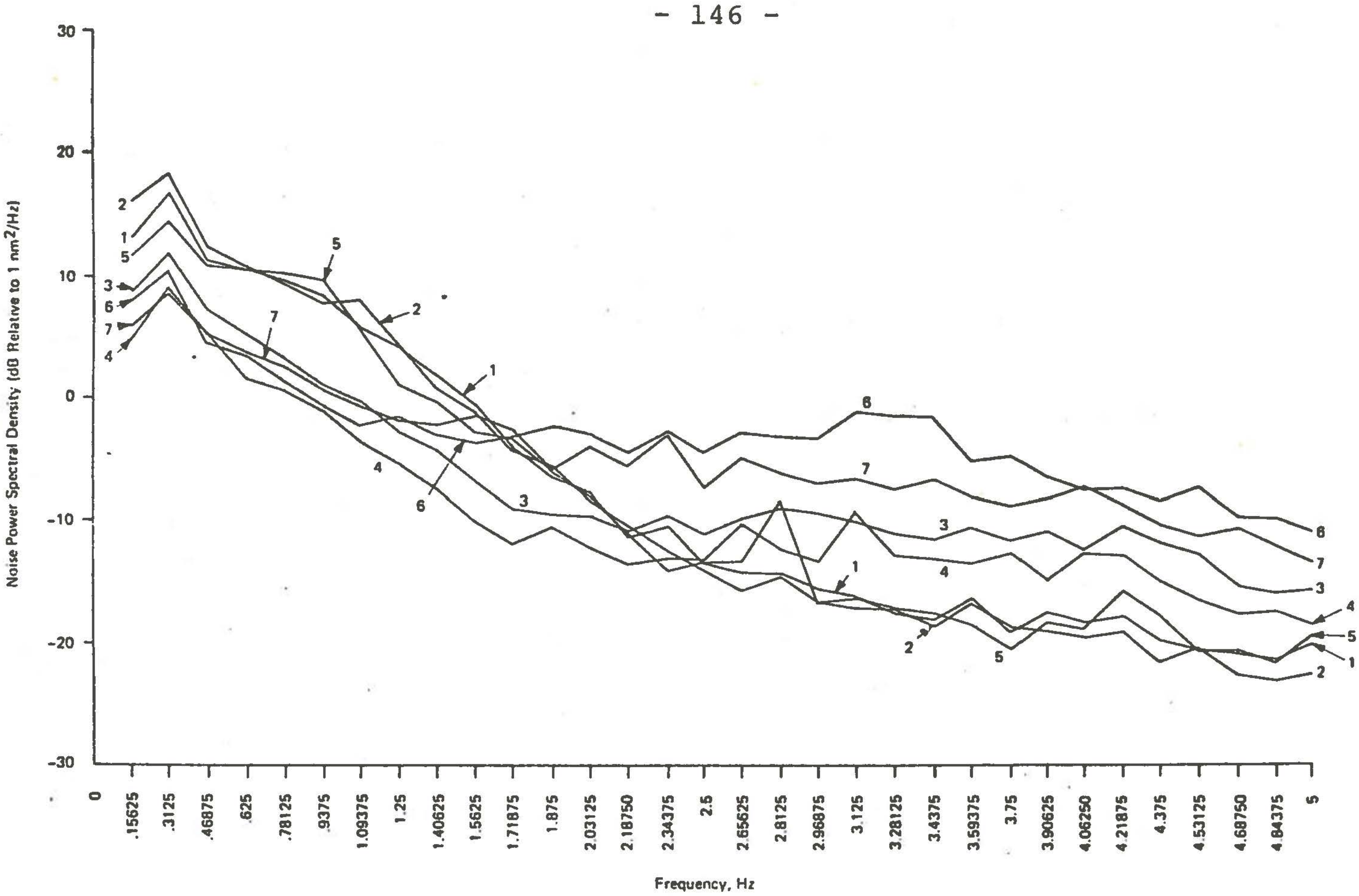

Fig 1. NORSAR Noise Power Spectral Density Functions

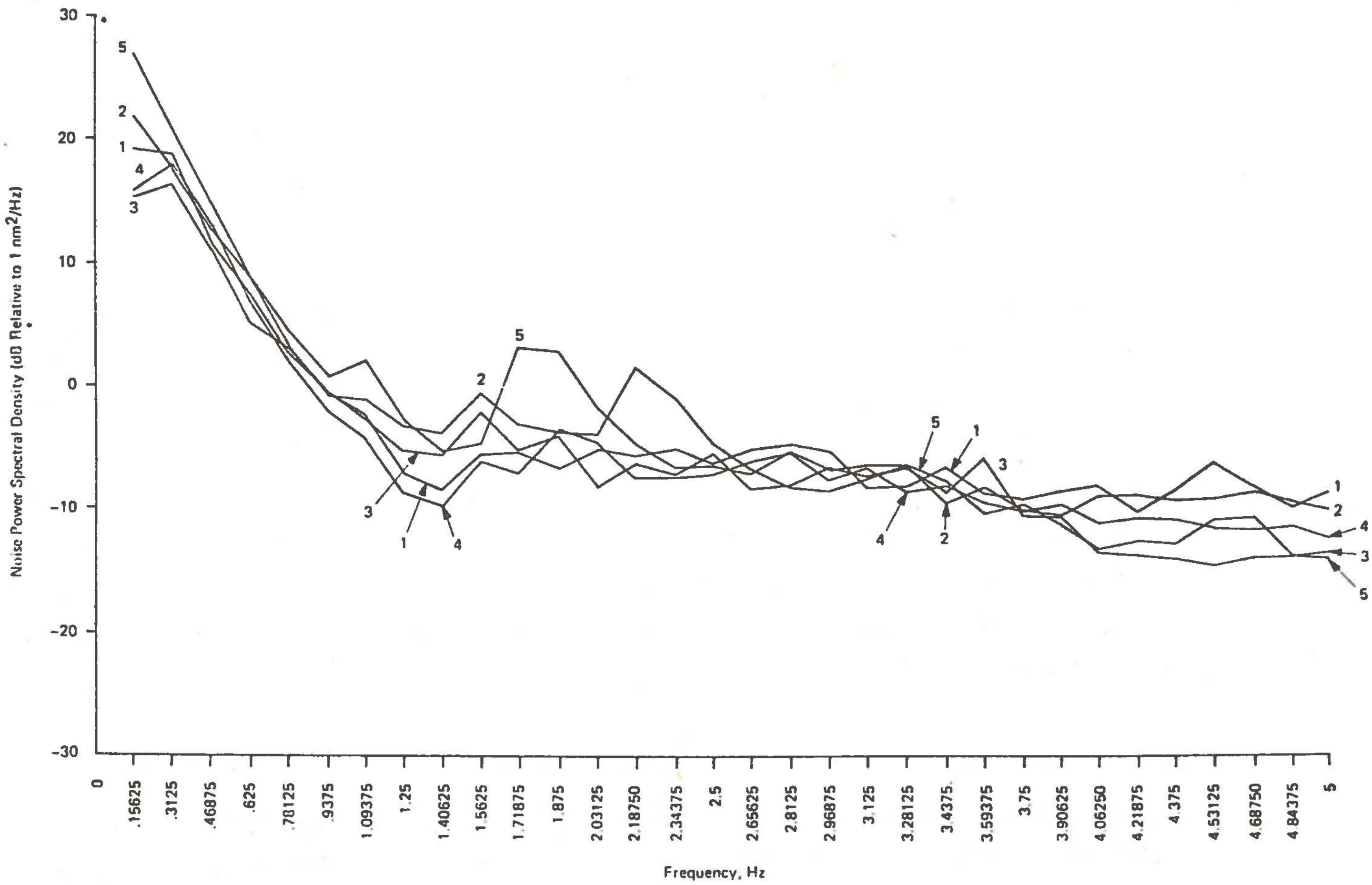

Fig 2. LASA Noise Power Spectral Density Functions

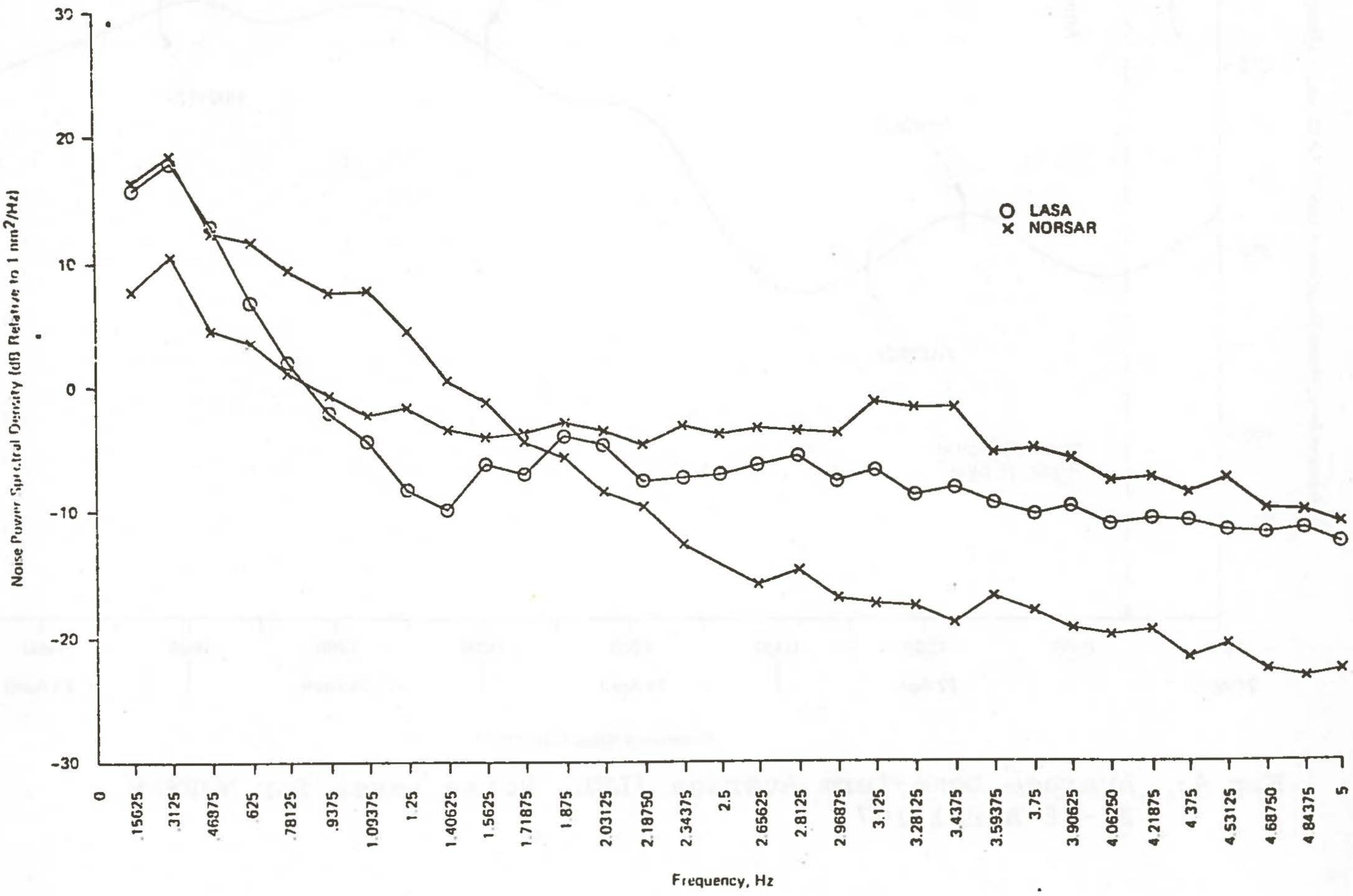

Fig 3. Selected NORSAR and LASA Noise Power Spectral Density Functions

0.9 to 3.5 Hz digital filter utilized in the Detection Processor at that time. The diurnal variations are somewhat significant at the beginning of the observation time interval, through approximately 1200 Z, 23 April, indicating the possibility that local winds at the array, although not reported as especially strong, might have been a significant contributing factor to the array noise during this time. Beginning during the morning of 23 April and continuing until the morning of 24 April there is a rise in the noise level which is considerably more significant than the earlier diurnal variations. This increased noise level continues throughout the day on 24 April, and begins to decrease during the morning of 25 April.

In order to obtain a better understanding of some of the causes for significant changes in the short-period seismic noise at NORSAR, particular attention was focused on the spectral characteristics of the noise and on the related meteorological phenomena

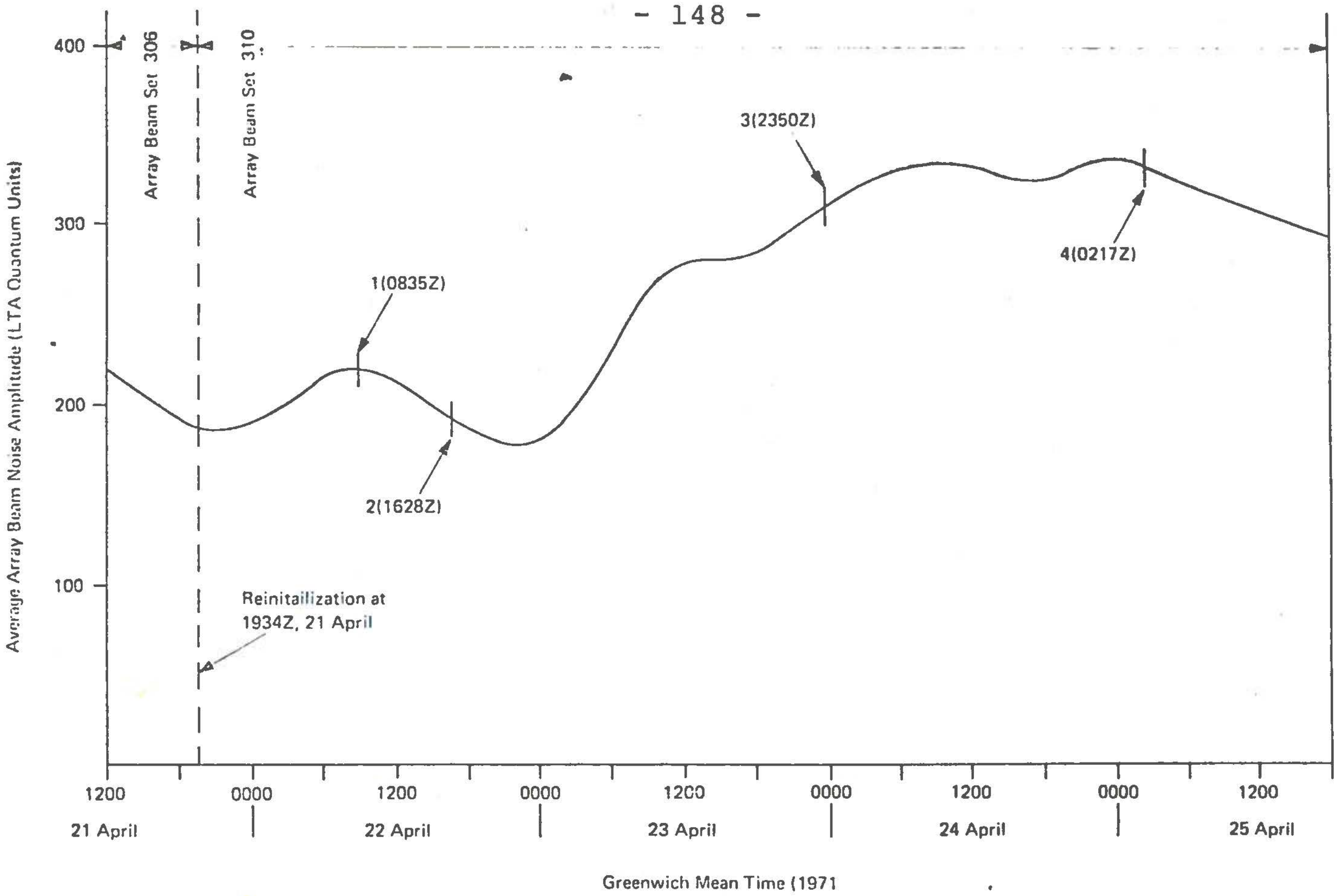

Fig 4. Average Long-Term Average (LTA) Noise Level for NORSAR 21-25 April 1971

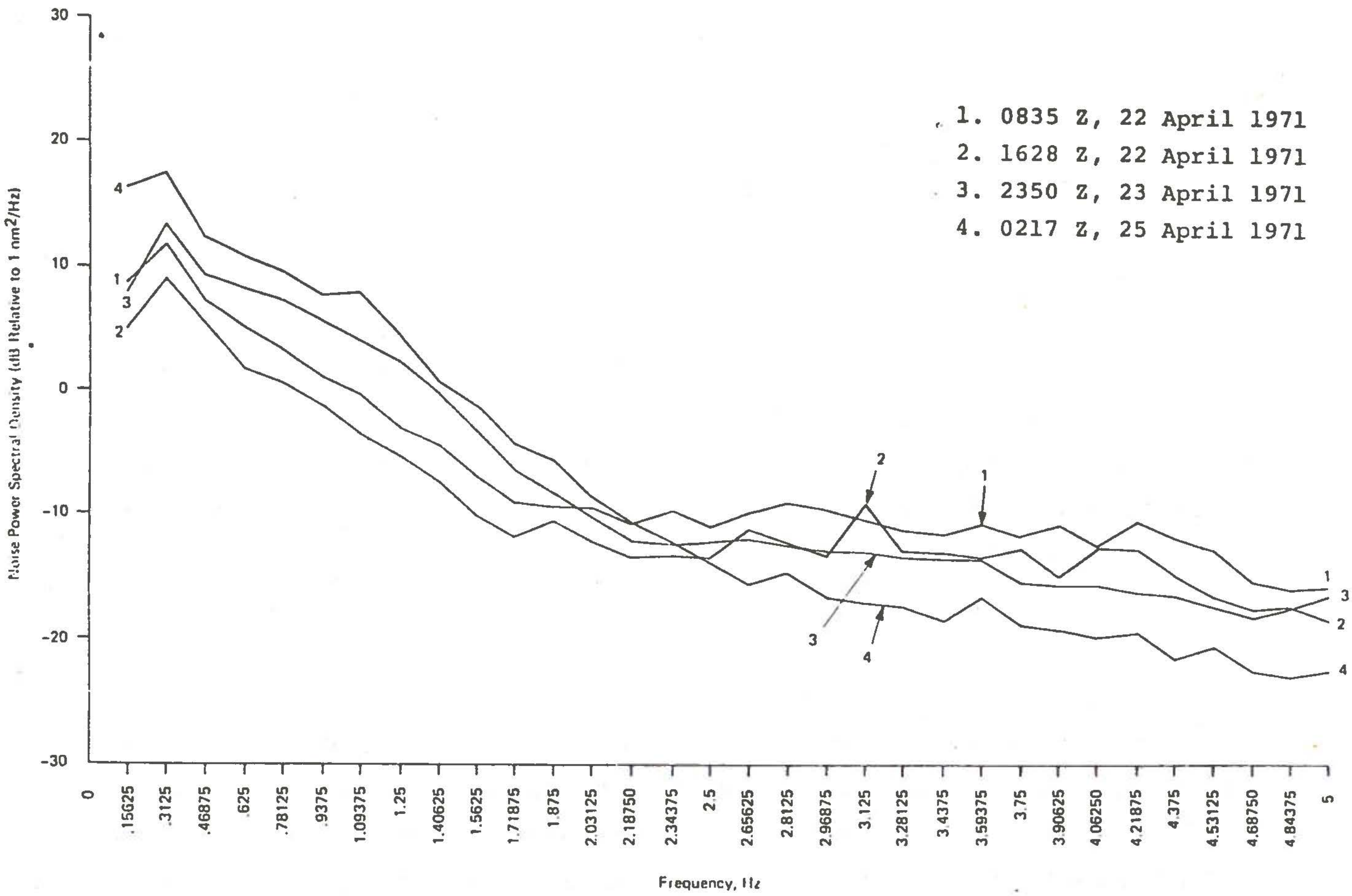

Fig 5. NORSAR Noise Power Spectral Density Functions, 22-25 April 1971

during this four-day period. The approximate times at which four of the spectral density functions were estimated are shown in Fig 4, and the corresponding spectral density functions are shown in Fig 5. Examination of the noise spectra over the 0.9 to 3.5 Hz filter passband shows a firm agreement with the corresponding average noise levels of Fig 4. The average noise levels shown in Fig 4 generally provide an indication of the behavior of the low frequency portion of the noise spectrum, say from 0.0 - 2.0 Hz. The higher frequency noise, say from 2.5 to 5.0 Hz, appears to decrease steadily during this period.

Fig 6 shows a portion of a U.S. National Oceanic and Atmospheric Administration Weather Chart for 0000 Z, 24 April 1971. NORSAR is indicated by a circle which is drawn approximately to scale. There is a fairly steep pressure gradient over the entire North Sea and a portion of the North Atlantic which is caused by one low pressure center over the English Channel and another one approximately 15° west of Scotland. This pressure gradient indicates the presence of a strong wind field over the area. The sequence of four-per-day U.S. NOAA Surface Weather Charts in Fig 7 shows that the pressure gradient over the North Sea (indicated by the reference area from 0° to 5° E. longitude and from 55° to 60° N. latitude) becomes steep between 1800 Z, 22 April and 0600 Z, 23 April. This gradient, and the corresponding wind field, have shifted direction by 1200 Z, 24 April, and have begun to decay by 1800 Z 24 April.

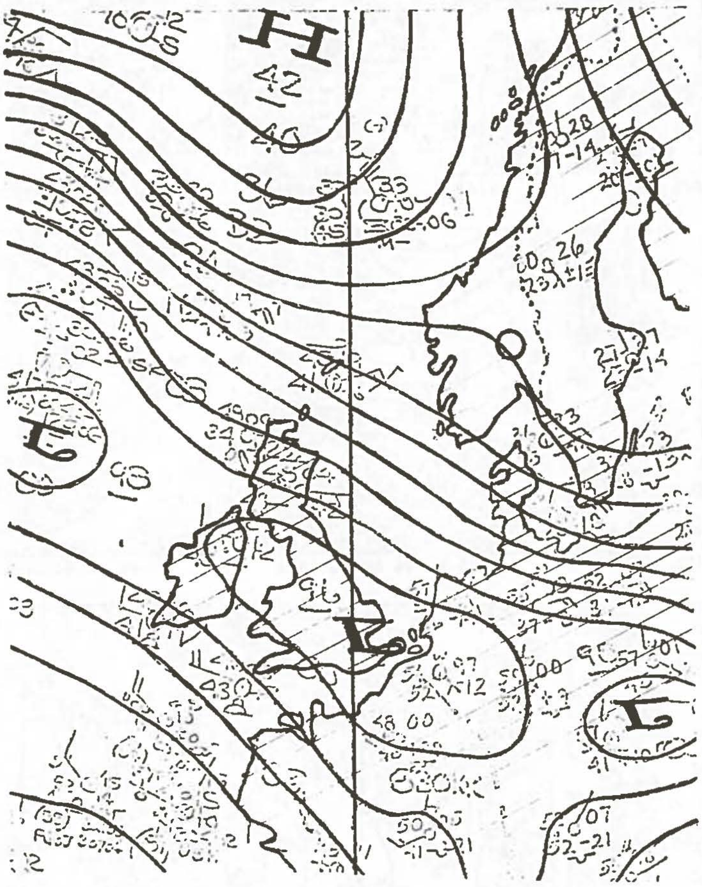

Fig 6. Portion of U.S. NOAA Surface Weather Chart, 0000 Z, 24 April 1971

Fig 7. Portion of National Oceanic and Atmospheric Administration Northern Hemisphere Surface Weather Charts, 22-25 April 1971 (Reference Area Coordinates: 0^{o}-5^{o} E Longitude; 55^{o}-60^{o} N Latitude) (Four millibar spacing between isobars)

Techniques which have been developed and automated by the U.S. Navy Fleet Numerical Weather Center for the analysis and prediction of sea-swell and storm waves use the following parameters, which all contribute positively in the above-described situation:

- Strength of wind (3-40 knots)
- Duration of wind in uniform direction (approximately 48 hours)
- Fetch of straight wind field over continental shelf (over 500 miles)
- Action of cold air on warmer water (see temperatures reported in Fig 7)

Therefore one possible explanation of the increased background noise level at NORSAR during this period is that microseisms caused by sea-swells in the North Sea and a portion of the North Atlantic, as well as surf noise along some portions of the Norwegian coast, were responsible. It should also be noted that the buildup and decay of sea-swells will generally lag the wind field cycle by several hours; for the case under discussion this lag appears to be on the order of six hours.

SIGNAL CHARACTERISTICS

For each signal waveform that has been analyzed, the signal-to-noise ratios of each of individual seismometer outputs in the case of Interim NORSAR data have been measured, together with the signal-to-noise ratio of the array beam. Under the assumption of unity signal coherence and zero noise coherence, and using the subarray weights which were utilized in the array beamforming process, the theoretical array beam signal-to-noise ratio has been computed. The beamforming loss for each event has also been computed in dB relative to the ideal, or theoretical, gain. These losses were then ordered numerically for the set of events, and plotted against the cumulative percent of total events. Fig 8 shows a smooth curve which was derived from the cumulative beam loss plot.

Since the assumption of negligible noise coherence among subarrays has been independently confirmed, the curve shown in Fig 8 may be interpreted as a cumulative plot of beamforming loss due primarily to NORSAR signal incoherence for the set of events tested, and secondarily to misalignment in the beamforming process due to sampling and residual delay errors. This plot indicates that the beamforming losses due to signal incoherence are less than 5.0 dB for 90 percent of the events, but that beamforming losses for some events exceed 6.0 dB.

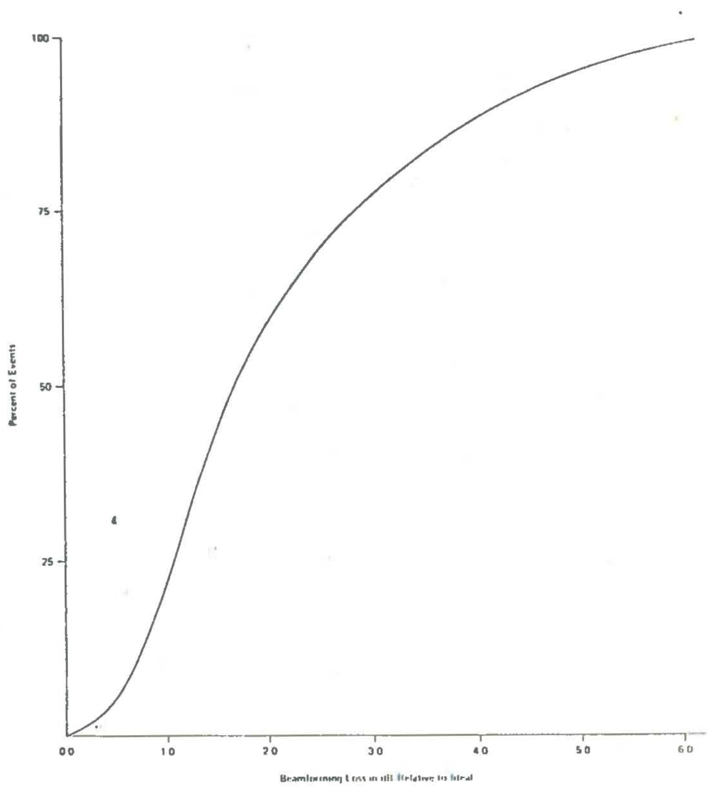

Fig 8. Cumulative Distribution of Beamforming Loss. Loss due to Signal Incoherence and Residual Misalignment

For each of the above-referenced 48 events processed by the full NORSAR system, in which all 22 NORSAR subarrays were utilized, the median subarray signal amplitude has been determined. Fig 9a is a plot of the individual subarray signal amplitudes in dB relative to the median amplitude for each event. In this and other parts of Fig 9, the channel numbers 1 through 22 correspond to subarrays 1A, 1B through 7B and 1C through 14C respectively. The vertical resolution of each of these plots is one dB; the number of multiple values which fall into the same resolution cell of the computer-printer plot is indicated by the integers two through nine followed by the letters of the English alphabet for integers above nine. The diamond-shaped brackets are centered at the median value, for each subarray channel.

Fig 9a shows that the spread of relative amplitudes for the various channels ranges from 10 to 20 dB, and that the medians vary between +2 dB and -3 dB. Therefore it appears that the relative amplitude response performance of the various subarrays over a large variety of events from various regions will tend to be uniform.

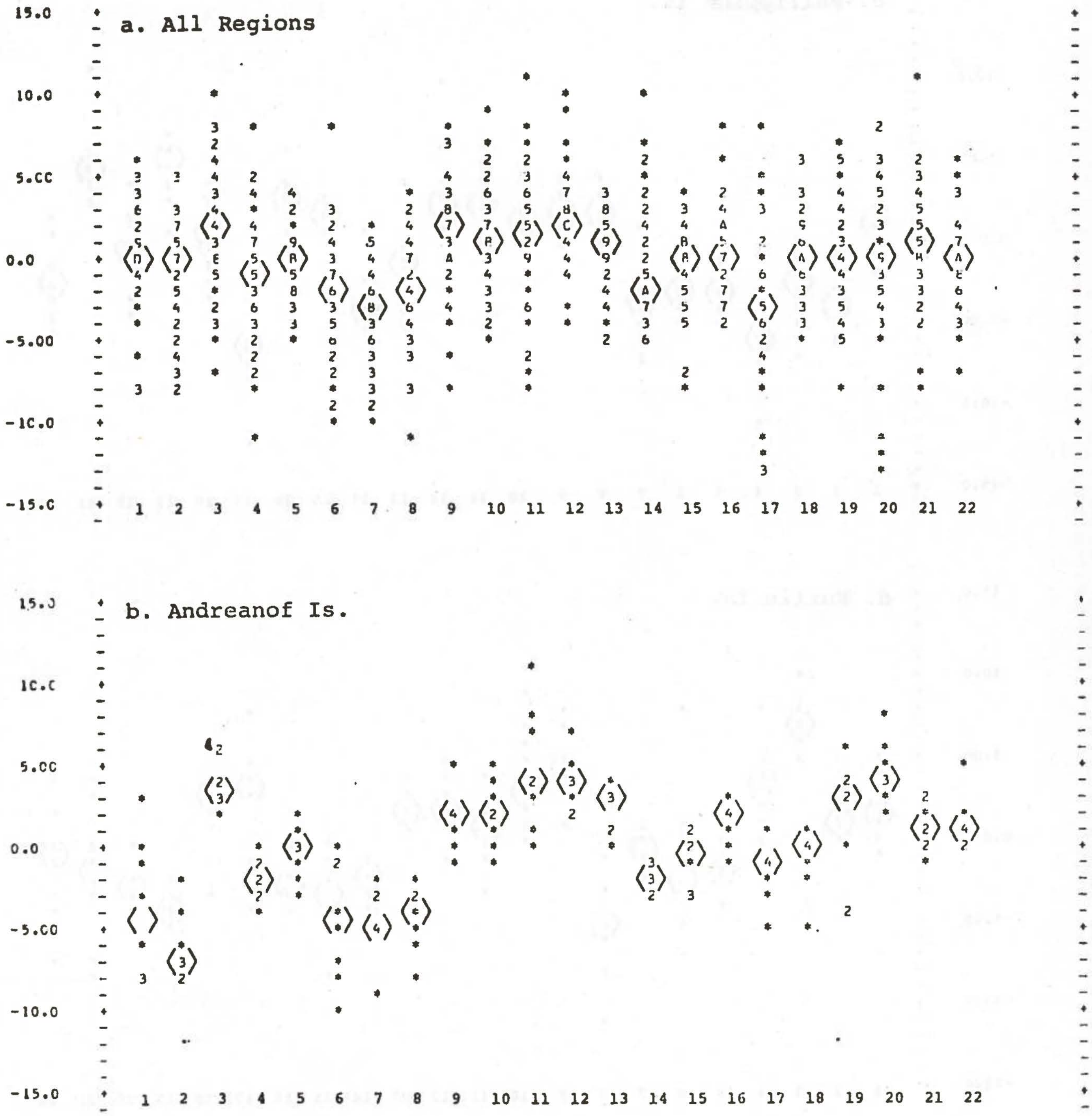

Fig 9a and b. Relative Subarray Amplitude Anomalies

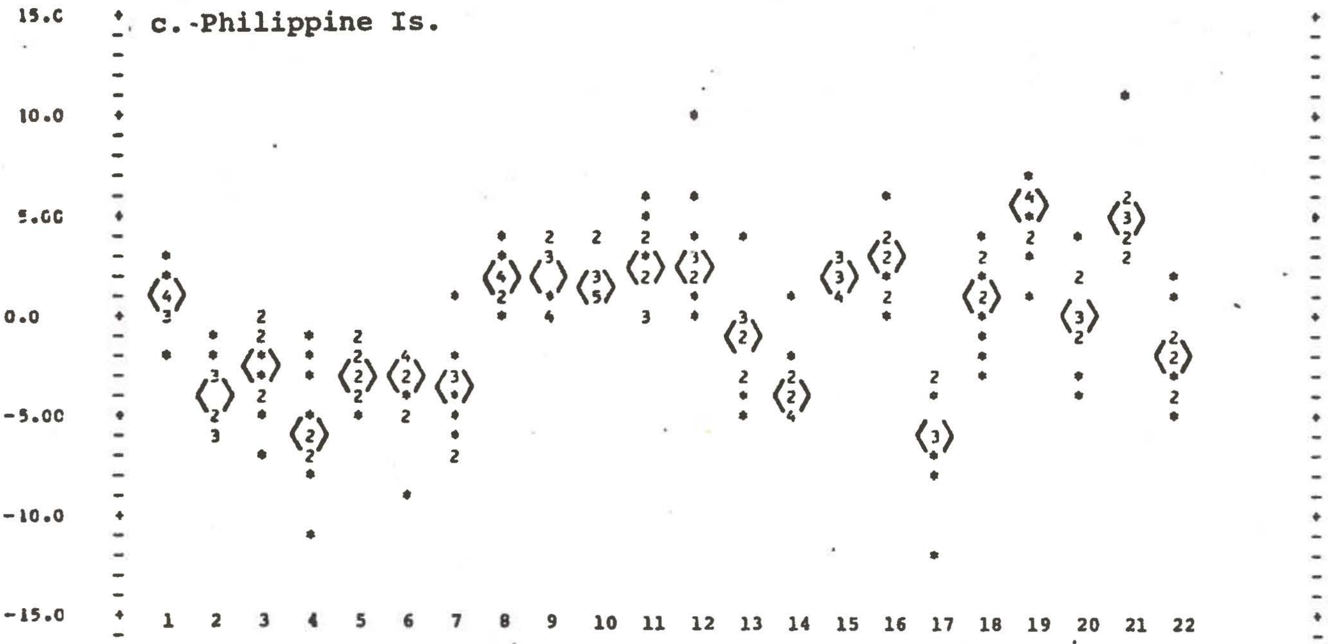

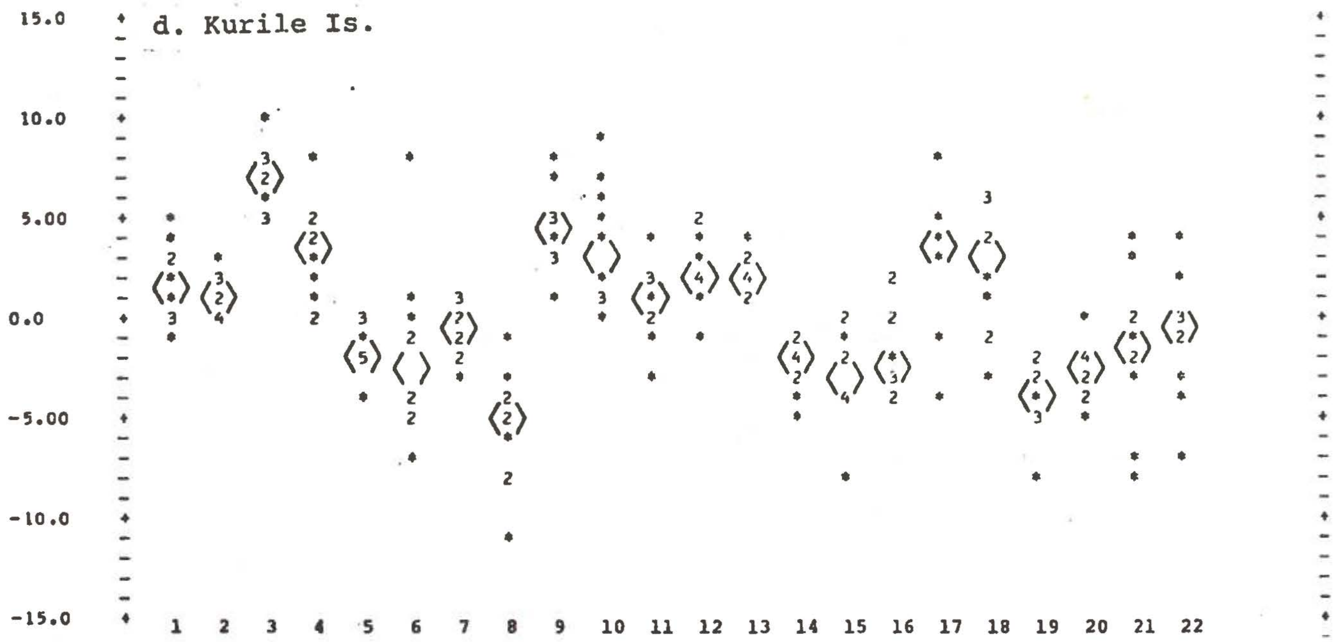

Fig 9c and d. Relative Subarray Amplitude Anomalies

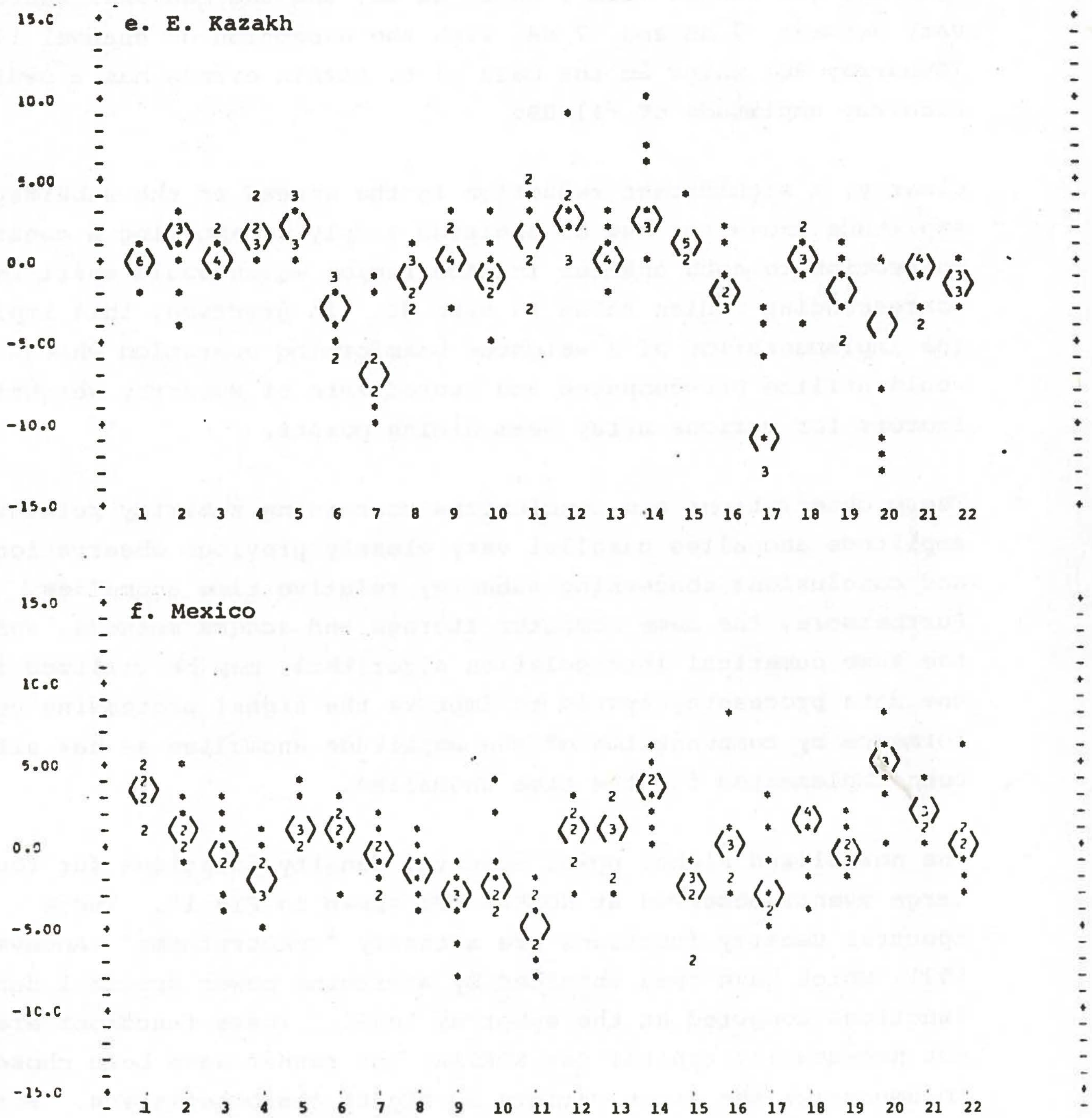

Fig 9e and f. Relative Subarray Amplitude Anomalies

However, when the events are grouped as a function of epicenter location, as shown in Fig 9b through 9f, it becomes clear that the relative subarray amplitude anomalies are quite predictable and repeatable. The spread in relative amplitudes for the various channels now ranges from 3 dB to 12 dB, and the medians generally vary between +7 dB and -7 dB, with the exception of channel 17 (Subarray 9C) which in the case of E. Kazakh events has a median subarray amplitude of -11 dB.

Clearly, a significant reduction in the spread of the subarray amplitude anomalies may be achieved simply by applying a constant correction to each channel in each region which would shift the corresponding median value to zero dB. In practice, this implies the implementation of a weighted beamforming operation which would utilize pre-computed and stored sets of subarray weighting factors for various array beam aiming points.

These observations and conclusions concerning subarray relative amplitude anomalies parallel very closely previous observations and conclusions concerning subarray relative time anomalies. Furthermore, the same computer storage and access methods, and the same numerical interpolation algorithms, may be utilized in the data processing system to improve the signal processing performance by compensation of the amplitude anomalies as has already been implemented for the time anomalies.

The normalized signal power spectral density functions for four large events observed at NORSAR are shown in Fig 10. These spectral density functions are actually "spectraforms" (Anonymous, 1971) which have been obtained by averaging power spectral density functions computed at the subarray level. These functions are not necessarily typical for NORSAR, but rather have been chosen to emphasize the great variety of signal characteristics. For example, most of the energy of event number 1 is restricted to the region below 1.25 Hz, while the spectrum for event number 2 peaks at approximately 3 Hz. Events numbered 3 and 4 are both from E. Kazakh, and both exhibit a characteristic notch in the spectrum near 1.5 Hz, which has been observed for all E. Kazakh events. Hence, certain spectral characteristics are repeatable as a function of event location, but it has also been observed that these spectral characteristics are sometimes altered considerably for relatively small changes in event location.

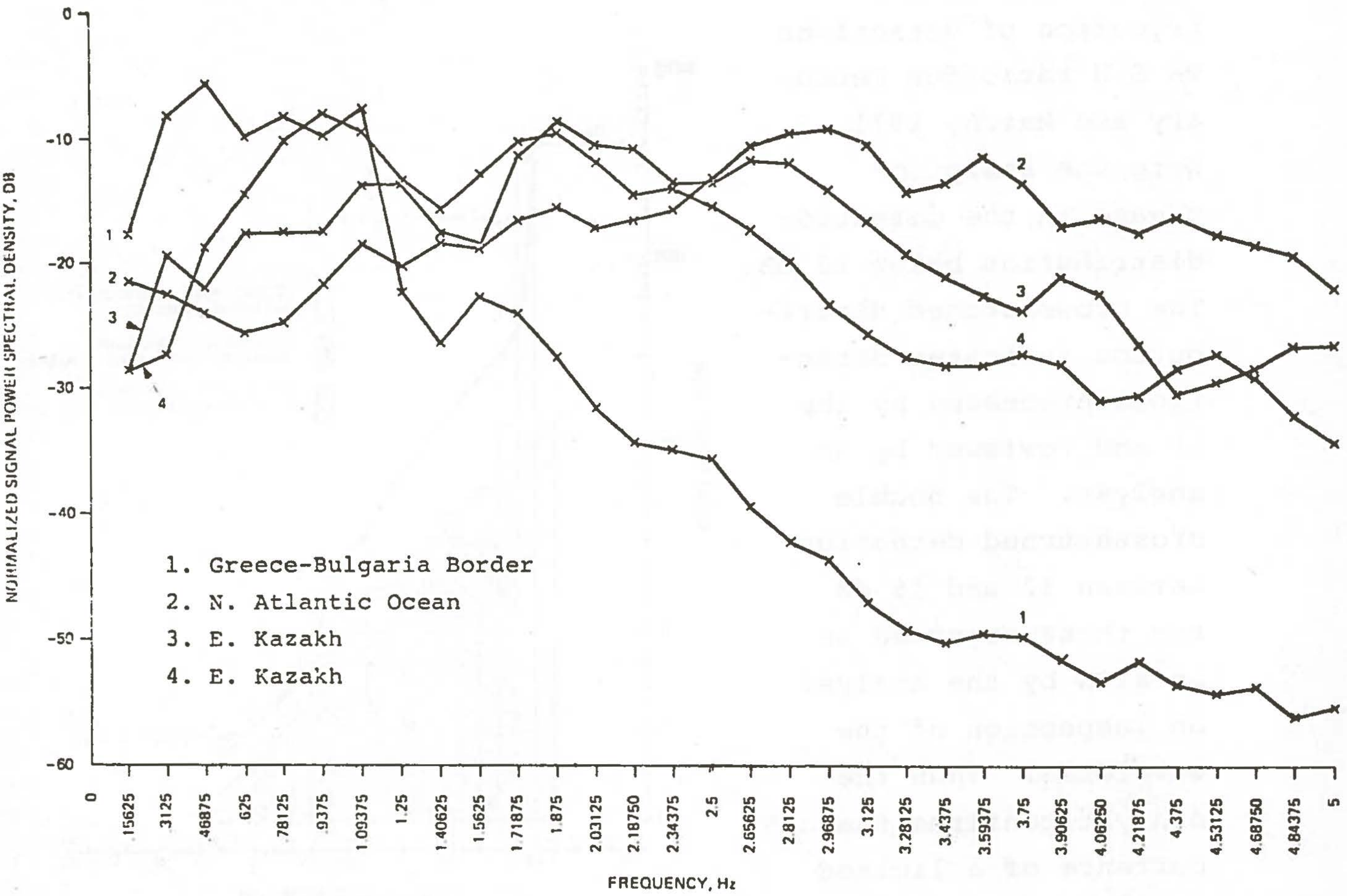

Fig 10. Selected NORSAR Signal Power Spectral Density Functions

SYSTEM PERFORMANCE ESTIMATES

Two approaches were used to estimate the Event Processor performance of the implemented NORSAR system. In the first, an internal system performance estimate was made by relating the observed distribution of detections, as a function of amplitude, to the expected distribution. This approach requires an assumption as to the validity of the detections observed and an estimate of the distribution of detectable signals. The second approach consists of measuring the noise distribution and inferring from it the Event Processor performance. An inherent danger in performance estimates based on internal system measurement is the possibility of unknown losses existing either within the system or within the data being processed. To estimate these losses, comparisons were made between the amplitude in the Detection Processor (DP), and the ratio of signal amplitude to period in the Event Processor (EP). In addition, a preliminary study of bias between NORSAR and the U.S. National Oceanic Survey magnitudes was performed.

Fig 11 shows the distribution of detections vs S/N ratio for February and March, 1971. Note the sharp increase in the detection distribution below 12 dB. The crosshatched distribution indicates detections processed by the EP and reviewed by an analyst. The double crosshatched detections between 12 and 16 dB are those rejected as invalid by the analyst on inspection of the waveforms. Thus the analyst confirms the occurrence of a limited number of false detections at this level and indicates no loss of valid signals. As an additional attempt to confirm the false detection distribution,

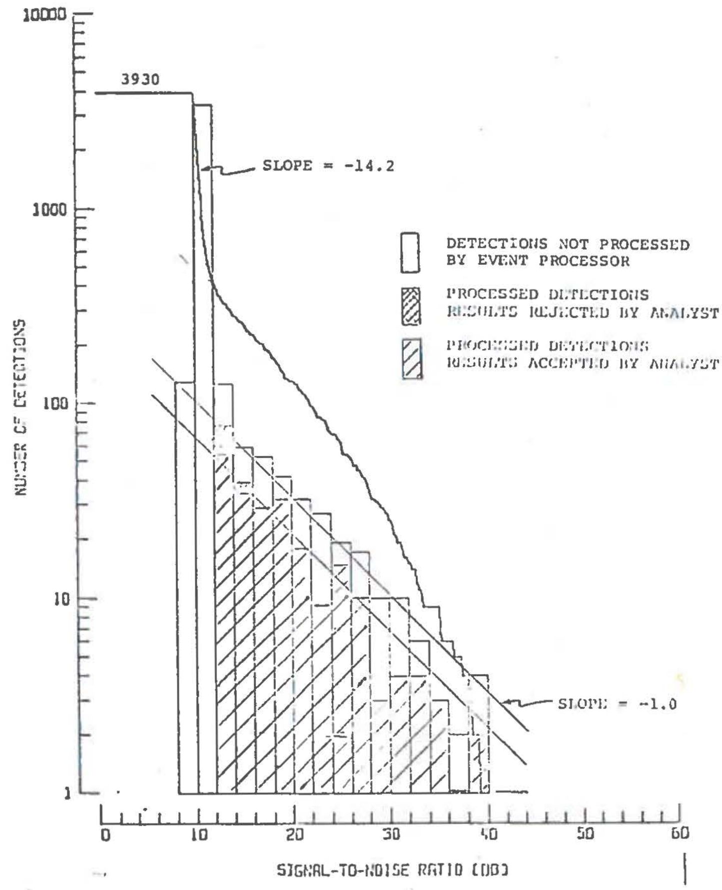

Fig 11. NORSAR Detection Distribution
Beam Set 306 (300 beams)
Selected Surveillance Partition
February 15 - March 31, 1971
Data Interval 37.0 Days

a subset of 29 beams deployed in aseismic regions was analyzed independently. Their distribution is shown in Fig 12. The expected reduction in high S/N detections has occurred and the steep slope for false detections is confirmed. Based on this evidence it was assumed that the incidence of false detections above 12 dB was sufficiently low to allow use of these detections to estimate the Event Processor performance. Fig 13 shows the data distribution by DP amplitude. The distribution of detections above the Event Processor threshold (S/N ≥ 12 dB) are indicated by the solid lines. The fall-off of detections below 2.0 nm indicates the loss in performance with the Event Processor operating at that level. To estimate the performance a logistic curve of the form

$$P(x) = \frac{1}{1+e^{-(\alpha+\beta x)}}$$

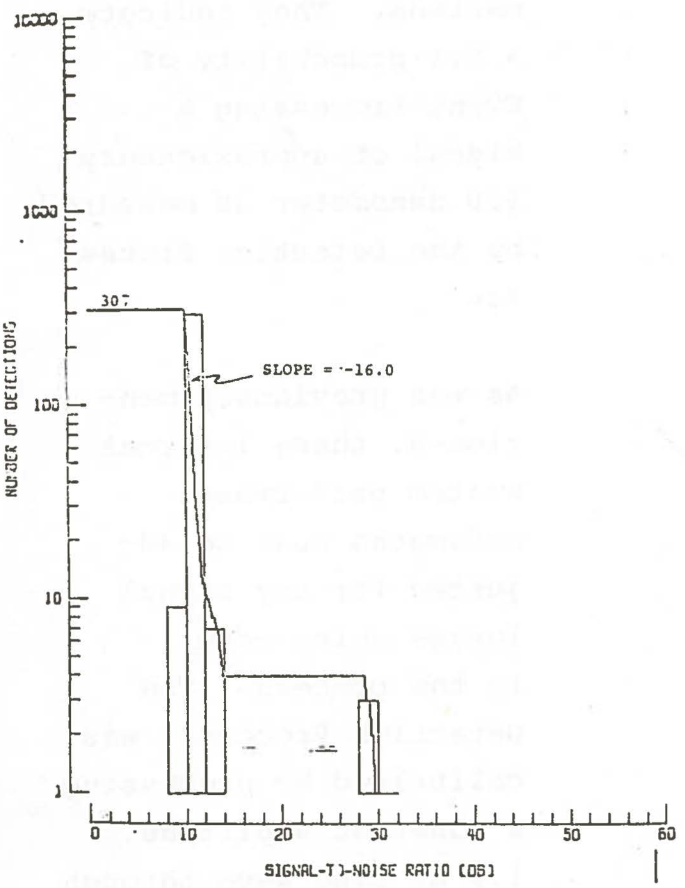

Fig 12. NORSAR Detection Distribution
29 Aseismic Beams
Selected Surveillance Partition
February 15-March 31, 1971
Data Interval 37.0 Days

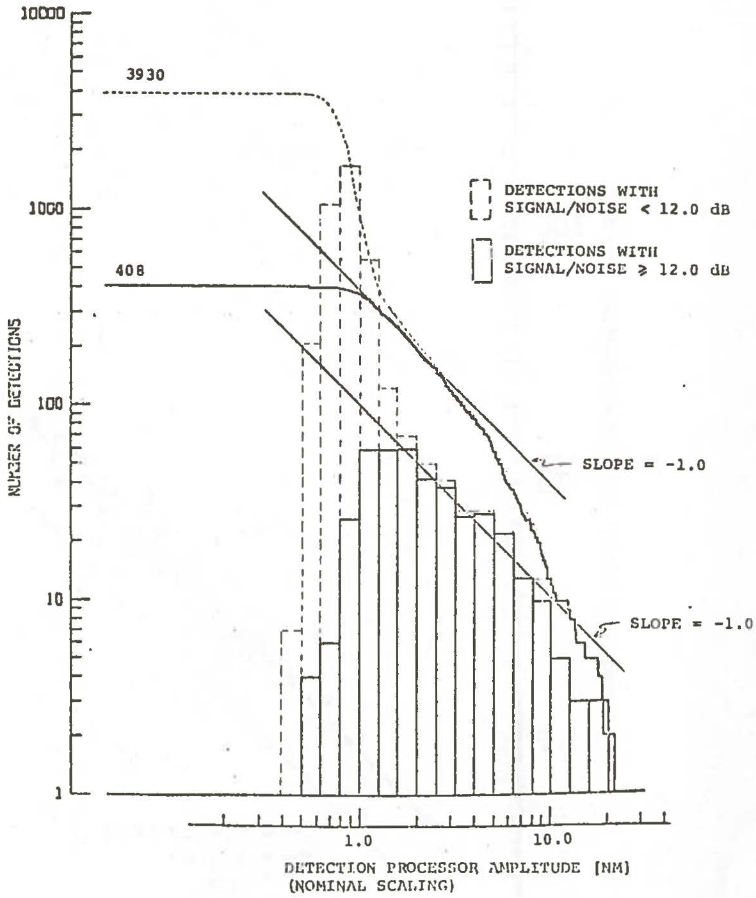

Fig 13. NORSAR Detection Distribution
Beam Set 306 (300 beams)
Selected Surveillance Partition
February 15-March 31, 1971
Data Interval 37.0 Days

was fit by least squares to the difference between the estimate of signal occurrence (a manually fit line with a slope of -1.0) and the observed detection distribution.

The second method uses the probability distribution of the seismic noise as observed by the system, shown at the left of the graph in Fig 15. To infer Event Processor performance from these distributions it is necessary to translate the curves by the Event Processor threshold. This threshold was operated at 12 dB (0.6 m_b units) in order to obtain an acceptable false detection rate in processing.

The independent estimates of capability derived from noise and detection distributions, the curves in the center of Fig 15, agree

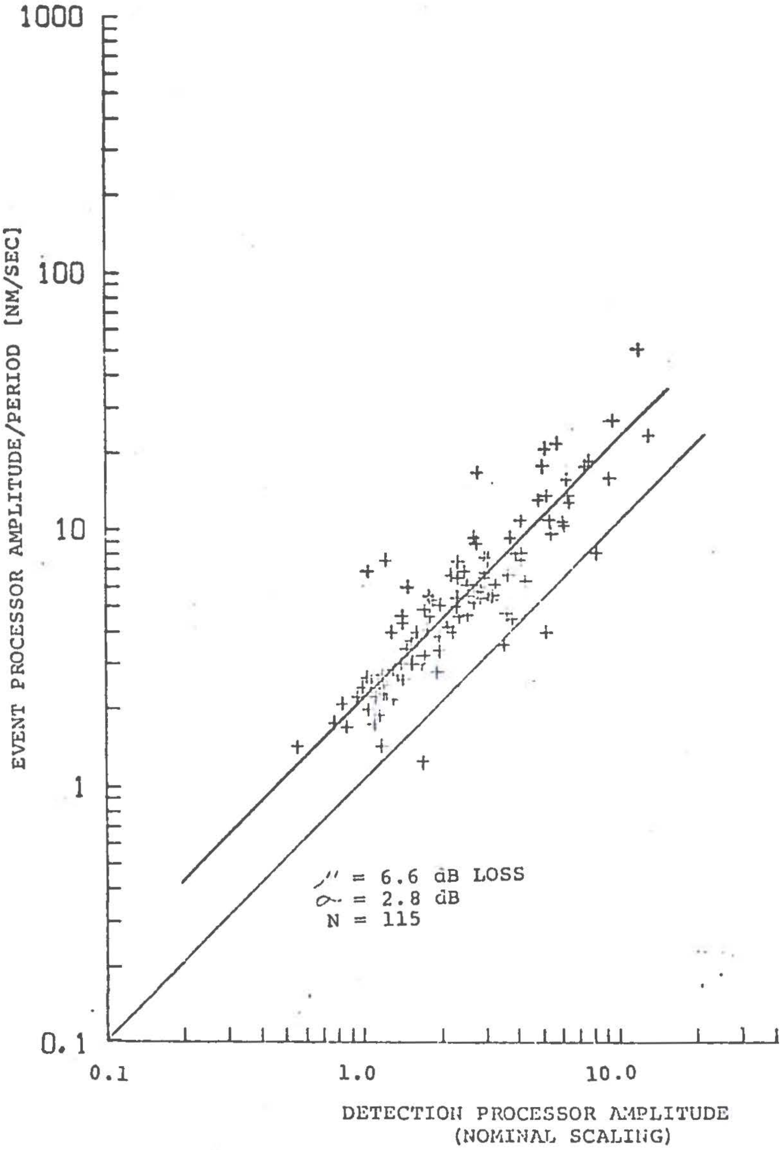

Fig 14. NORSAR System Scaling
Selected Surveillance
Partition
February - June 1971

very well for both periods. They indicate a 50% probability of Event Processing a signal of approximately 1.0 nanometer as measured by the Detection Processor.

As was previously mentioned, these internal system performance estimates must be adjusted for any signal losses which occur in the process. The Detection Processor was calibrated by processing a constant amplitude, 1.0 Hz sine wave through the digital system, assigning the same delays as were used in the beamforming process. When the system operates on actual seismic signals, additional losses are encountered. Such losses are due to beam missteering, time delay errors, quantization effects, etc. To estimate these losses empirically, a set of 115 processed signals was selected and the relationship between the DP amplitude and EP amplitude/period was obtained. A mean loss of 6.6 dB (0.33 m_b units) with a standard deviation of 2.8 dB was observed (Fig 14). This estimate of losses in the Detection Processor was used to construct the set of performance curves shown on the right of Fig 15. In addition to adding the mean loss to each curve, the variance of the loss estimate and the variances observed in each probability distribution were summed and new performance estimates were plotted assuming that a normal distribution would result. It should be noted that a portion of the

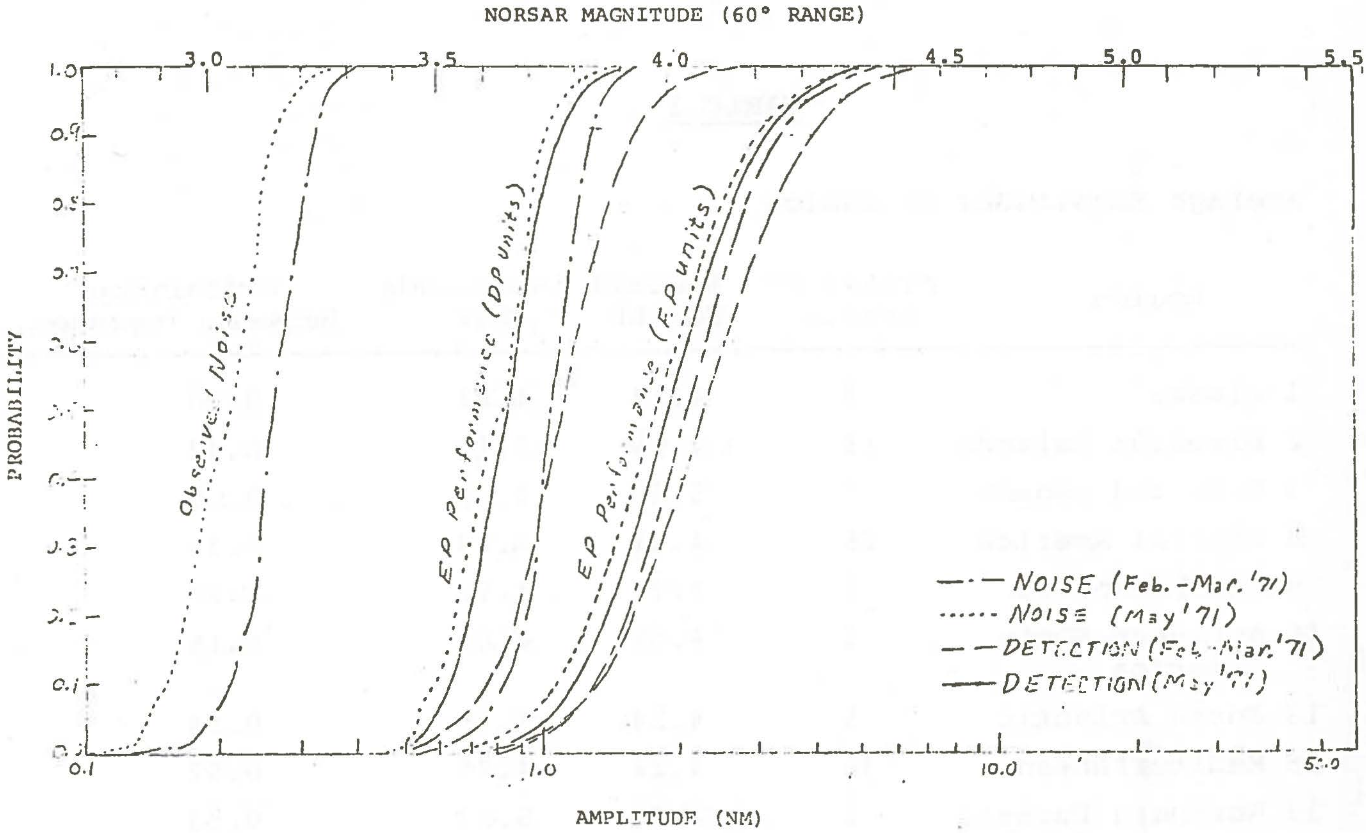

Fig 15. NORSAR Event Processor Performance

indicated losses can be recovered by improvement in the parameters of the present process; e.g., delay anomalies, beam deployment, filtering. Investigation into the specific causes of these losses is continuing along with development of the data base required to improve the beam delays. The curves to the right of Fig 15 give our estimate of the Event Processor performance as it was operated during the early part of 1971. They indicate 50% probability of processing a signal of approximately 2.0 nm/sec as measured by the NORSAR Event Processor. A magnitude scale is shown at the top of the graph to illustrate the performance at 60° range. To discuss system performance in relation to an external determination of event magnitude, a preliminary study of NORSAR vs U.S. NOS magnitudes was performed. The analysis of magnitude determinations for 245 events processed by the NORSAR system and reported by the U.S. NOS indicates substantial bias in the NORSAR estimates (see Table 1). Overall these data indicate that NORSAR magnitude estimates are biased low by 0.29 magnitude units. Significant regional biases are also indicated.

TABLE 1

Average Magnitudes by Region

Region	Number of Events	Average NORSAR	Magnitude C&GS	Difference Between Averages
1 Alaska	5	4.14	4.44	0.30
2 Aleutian Islands	18	4.69	5.12	0.43
3 U.S. and Canada	2	5.50	5.60	0.10
8 Central America	18	4.61	4.93	0.32
9 Caribbean Sea	1	4.70	4.90	0.20
10 Northern South America	5	4.52	4.68	0.16
13 North Atlantic	5	4.24	4.78	0.54
18 Mediterranean	30	4.24	4.76	0.52
19 Northern Eurasia	3	4.70	5.23	0.53
20 South Central Asia	38	4.80	5.08	0.28
21 Northern Indian Ocean	3	4.70	5.13	0.43
24 Java Trench, Philippines	41	4.84	5.18	0.34
25 Japan, Ryukyu Islands	37	4.74	4.81	0.07
26 Kurils, Hokkaido, Kamchatka	31	4.77	4.83	0.06
27 Marianas	7	4.59	5.07	0.48
28 New Guinea, Coral Sea	1	4.40	4.70	0.30
All Regions	245	4.66	4.95	0.29

Standard Deviation 0.48

Standard Deviation After Removing Regional Biases 0.36

REFERENCES

1. Anonymous, 1972a: Integrated Seismic Research Signal Processing System, IBM Final Technical Report, Contract F19628--68-C-0400, Appendix I. To be published.

2. Anonymous, 1972b: Integrated Seismic Research Signal Processing System, IBM Ninth Quarterly Technical Report, Contract F19628-68-C-0400, November 1970, Appendix V. To be published.

3. Anonymous, 1972c: Integrated Seismic Research Signal Processing System, IBM Final Technical Report, Contract F19628-68-C-0400, Appendix III. To be published.

4. Anonymous, 1968: Semiannual Technical Summary on Seismic Discrimination, Lincoln Laboratory, 30 June 1968, Section II.

5. Anonymous, 1971: Semiannual Technical Summary on Seismic Discrimination, Lincoln Laboratory, 30 June 1971, Section III-B.

6. M. Nafi Toksöz: Amplitude Anomalies and Signal-to-Noise Characteristics of NORSAR, preliminary draft.